

PAPER

Diffraction patterns of amorphous materials as a series expansion of neighbor distribution functions

To cite this article: M Micoulaut 2019 *J. Phys.: Condens. Matter* **31** 285402

View the [article online](#) for updates and enhancements.



IOP | ebooks™

Bringing you innovative digital publishing with leading voices to create your essential collection of books in STEM research.

Start exploring the collection - download the first chapter of every title for free.

Diffraction patterns of amorphous materials as a series expansion of neighbor distribution functions

M Micoulaut 

Sorbonne Université, CNRS, Laboratoire de Physique Théorique de la Matière Condensée,
4 Place Jussieu, 75252 Paris Cedex 05, France

E-mail: mmi@lptmc.jussieu.fr

Received 9 January 2019, revised 20 March 2019

Accepted for publication 1 April 2019

Published 30 April 2019



Abstract

An exact analytical expression for the static structure factor $S(k)$ in disordered materials is derived from Fourier transformed neighbor distribution decompositions in real space, and permits to reconstruct the function $S(k)$ in an iterative fashion. The result is successfully compared to experimental data of archetypal glasses or amorphous materials (GeS_2 , As_2Se_3 , GeTe), and links quantitatively knowledge of structural information on short and intermediate-range order with the motifs found on the diffraction patterns in reciprocal space. The approach furthermore reveals that only a limited number of neighbor shells is sufficient to reasonably describe the structure factor for $k > 2 \text{ \AA}^{-1}$. In the limit of the high momentum transfer, the oscillation characteristics of the interference function are related with new informations on the short-range order of disordered materials.

Keywords: glasses, structure, diffraction, molecular simulations

(Some figures may appear in colour only in the online journal)

1. Introduction

Diffraction methods form the basis of our common understanding of materials. The determination of crystal structures has provided a foundation for considerable characterization of chemical bonding, cohesion, and functionalities in solid- or liquid-state science with applications in e.g. physico-chemistry, biology and geology. In contrast to crystals which display well-defined diffraction patterns and sharp Bragg peaks induced by the periodic arrangement of atoms, glasses and liquids exhibit broad and diffuse peaks that result from their intrinsic disordered structure. For such materials and with changing momentum transfer k , there have been many attempts to extract from the relevant resulting coherent diffraction function, that is, the static structure factor $S(k)$, information on short- (SRO) and intermediate-range order (IRO) and a conventional means uses probabilistic atomic distribution functions to infer the microscopic structure [1].

Within this framework, the key quantity is the pair correlation function $g(r)$ which measures the probability of finding

an atom at a position r relative to a reference atom taken to be at the origin [2]. Relating in detail the real space structure properties encoded in $g(r)$ and the shape and peak positions or amplitudes of the measured $S(k)$ remains a challenging task but has inspired a certain recent number of insightful contributions in the field [3–6], many years after the early attempts of Warren [7] and Bernal [8]. In fact, only certain specific signatures can be detected and related to some structural features. The first sharp diffraction peak (FSDP) at low momentum transfer ($k \simeq 1 \text{ \AA}^{-1}$) reveals for instance some ordering at intermediate length scales [9, 10] that might manifest in e.g. voids and depends on pressure and temperature. Similarly, principal peak (PP) characteristics are thought to be linked to the presence of extended range order [11, 12]. Such features continue, however, to be discussed given that the established correlations remain essentially at a qualitative level and are largely material dependent.

Here we show that with the assistance of computer simulated structural models of glasses, the decomposition into neighbor distribution functions in real space permits to reconstruct as a

series expansion the structure factor, and an exact analytical expression for $S(k)$ is obtained from Fourier transformation. Such expressions exist for imperfect crystals with weak disorder [13] but here it is the first time that a similar approach is used for disordered materials such as glasses (see also [14]). This not only links quantitatively information on ordering with characteristics of the structure factor $S(k)$, but also reveals what aspects of structure directly influence typical features observed experimentally at different momentum transfer. While accurate computer-based model structures can permit the calculation of any structural property in reciprocal space, the present method permits to analyze the diffraction patterns of materials for which MD derived structural models are either unavailable or only partially in agreement with experiments. Based on the analysis given below, this sort of reverse analysis using $S(k)$ as a series expansion now provides some hints for an increased analysis of experimental structure factors.

We first concentrate on the amorphous system As_2Se_3 before investigating the degree of generality of the findings on other chalcogenide glasses such as GeS_2 and GeTe . The high k limit of the analytical expression leads to another exact result that permits to fully characterize the typical oscillations observed in the experimental interference function $I(k) = k[S(k) - 1]$. We then examine a certain number of glasses that have been investigated experimentally.

2. Theory

2.1. The interference function as a series expansion

The starting point of the approach uses the definition [2] of the structure factor given by:

$$S(k) - 1 = 4\pi\rho_0 \int_0^\infty r^2 [g(r) - 1] \frac{\sin(kr)}{kr} dr \quad (1)$$

where ρ_0 is the atomic number density. The system is considered as being isotropic and homogeneous so that integration can be applied on the vector norms $r = |\mathbf{r}|$ only, this being particularly adapted for disordered systems simulated in a cubic box of size L down to wave number somewhat larger than $2\pi/L$.

We propose that the pair distribution function $g(r)$ can be decomposed into a series of neighbor distribution functions $v_n(r)$ ($1 \leq n \leq N$) as exemplified in different liquids and glasses [15–17] (figure 1). For each atom, distributions are constructed from molecular dynamics (MD) based trajectories by sorting the neighbours according to the bond length. We assume that such distribution functions can be reconstructed by Gaussians $u_{nm}(r)$ with amplitudes A_{nm} , mean distances (first moments) r_{nm} and variances σ_{nm}^2 . Note that the index ($M \geq m \geq 1$) signals that up to M Gaussian functions might be used to fit a given distribution function $v_n(r) = \sum_m^M u_{nm}(r)$. In the forthcoming, applications to different systems have shown that not more than $M = 3$ Gaussians are needed to reproduce accurately a function $v_n(r)$ calculated from the MD simulations, and in most of the situations $M = 1$ is sufficient, especially at short distance.

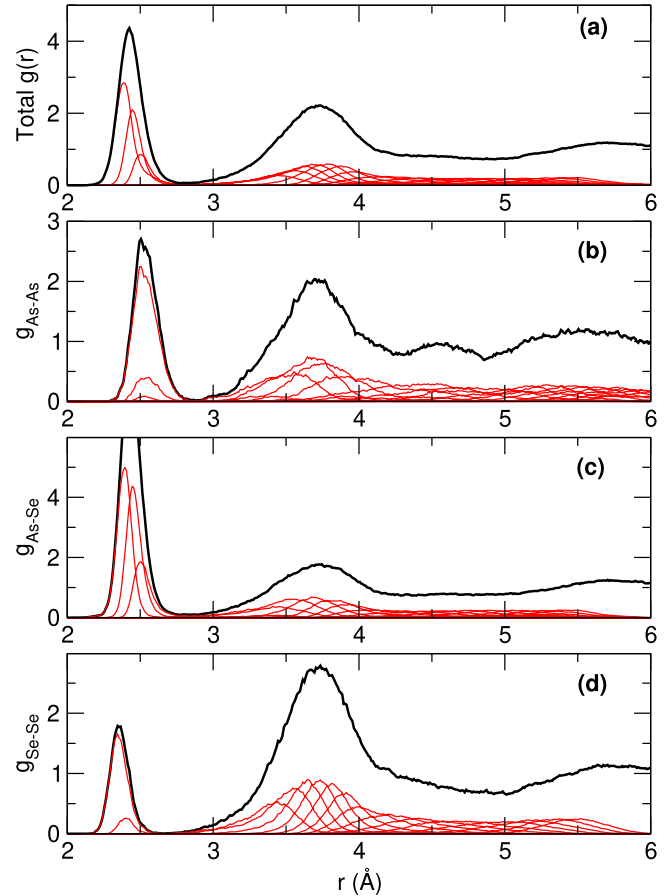


Figure 1. Total [18] (a) and partial neighbor ((b)–(d)) decomposition (red curves) in amorphous As_2Se_3 , together with the total or partial pair correlation functions (black lines).

It is possible to extend the approach from a monatomic material in which all the atoms are chemically identical to a polyatomic system where (neutron or x-ray) scattering depends on the atomic sites occupied by a given chemical species. In this case, for an atomic pair $i - j$, neighbor distribution functions v_n^{ij} can be defined in the same way as above with corresponding Gaussian parameters, and these serve to construct partial pair correlation functions $g_{ij}(r)$ (figures 1(b)–(d)). The resulting functions pair correlation function $g(r)$ then writes:

$$g(r) = \frac{\sum_{ij} c_i c_j f_i f_j g_{ij}(r)}{\sum_{ij} c_i c_j f_i f_j} \quad (2)$$

with f_i being either equal to the neutron scattering length ($f_i = b_i$ in case of a comparison with neutron scattering experiments) or to the x-ray form factor (often taken as $f_i = Z_i$ the atomic number, albeit valid only at large beam energies) when a comparison with x-ray results is to be performed. In the forthcoming, we will restrict our study to the total pair correlation function in order to compare directly with a larger number of experiments.

Using such distributions, a direct calculation shows that equation (1) can be exactly computed and leads to the interference function:

$$\begin{aligned}
I(k) &= k[S(k) - 1] = \sum_{n=1}^N I_n(k) \\
&= 4\pi\rho_0 \sum_{n,m}^{N,M} A_{nm} \sigma_{nm}^2 \sqrt{2} e^{-r_{nm}^2/2\sigma_{nm}^2} \left[r_{nm} L_{nm} + k\sigma_{nm}^2 V_{nm} \right]
\end{aligned} \quad (3)$$

where V_{nm} and L_{nm} represent the Voigt functions [19, 20] for the m th Gaussian component associated to the neighbour distribution $v_n(r)$:

$$\begin{aligned}
L_{nm} &= L_{nm} \left(\frac{k\sigma_{nm}}{\sqrt{2}}, -\frac{r_{nm}}{\sigma_{nm}\sqrt{2}} \right) \\
&= \frac{1}{\sqrt{\pi}} \int_0^\infty e^{-t^2/4+r_{nm}t/\sigma_{nm}\sqrt{2}} \sin\left(\frac{k\sigma_{nm}}{\sqrt{2}}t\right) dt
\end{aligned} \quad (4)$$

$$\begin{aligned}
V_{nm} &= V_{nm} \left(\frac{k\sigma_{nm}}{\sqrt{2}}, -\frac{r_{nm}}{\sigma_{nm}\sqrt{2}} \right) \\
&= \frac{1}{\sqrt{\pi}} \int_0^\infty e^{-t^2/4+r_{nm}t/\sigma_{nm}\sqrt{2}} \cos\left(\frac{k\sigma_{nm}}{\sqrt{2}}t\right) dt
\end{aligned} \quad (5)$$

V_{nm} and L_{nm} being also equal to the real and imaginary parts of the Fadeeva function $w_n(z)$ [20] with $z = \frac{k\sigma_{nm}}{\sqrt{2}} - \frac{ir_{nm}}{\sigma_{nm}\sqrt{2}}$ defined from the complex error function:

$$w_n(z) = e^{-z^2} \left[1 + \frac{2i}{\sqrt{\pi}} \int_0^z e^{t^2} dt \right]. \quad (6)$$

In the thermodynamic limit, equation (3) is an exact result and its validity as well as the convergence properties can be checked for a variety of disordered systems with increasing N .

2.2. Model details

For the analysis and application of equation (3), three amorphous materials have been investigated. All result from first principles molecular dynamics simulations that build on density functional theory (DFT) encoded in the Car–Parrinello scheme [21]. The electronic structure of the all systems evolved self-consistently during the motion using a general gradient approximation (GGA) for the exchange and correlation parts of the total energy. Valence electrons were treated explicitly, in conjunction with normconserving pseudopotentials to account for core-valence interactions. The wave functions were expanded at the Γ point of the supercell and the energy cutoff was set for all to 20 Ry. Quenching procedures to obtain the amorphous state can be found in the relevant [18, 22–24]. For all, the trajectory has been integrated with a time step of 0.12 fs.

2.2.1. As_2Se_3 . The amorphous As_2Se_3 system consists in $N = 200$ atoms that are simulated with a Becke, Lee, Yang and Parr (BLYP) exchange correlation functional [25]. Details on model generation, comparison with experiments and structural analysis (bond distances, coordination numbers, ring statistics, topological constraints ...) can be found in [18, 22, 26, 27]. The general outcome of these studies is an improved agreement with experimental structure functions ($S(k)$, $g(r)$),

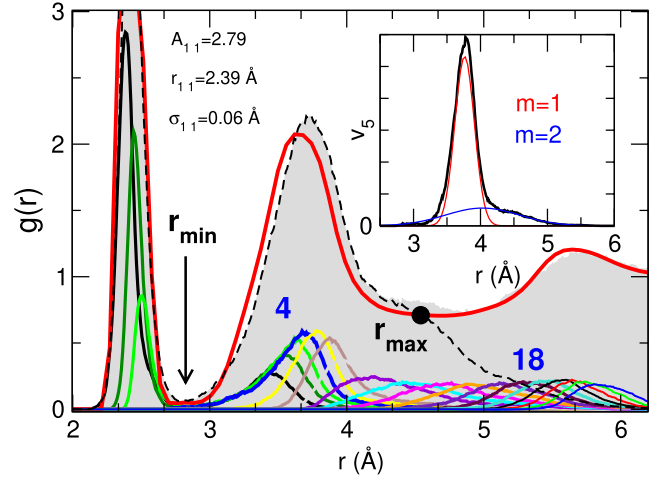


Figure 2. Calculated total pair correlation function $g(r)$ (gray) of simulated amorphous As_2Se_3 [22] together with its decomposition into neighbor distribution functions $v_n(r)$ (colored curves, up to $n = 18$) and corresponding results from neutron diffraction (red curve, [31]). The broken black curve corresponds to $\sum_{n=1}^{10} v_n(r)$ and defines a distance r_{\max} for a given N (here $N = 10$). The inset shows v_5 and its decomposition into $M = 2$ Gaussians. The distance r_{\min} defines the minimum of $g(r)$ and is used for the determination of a coordination number.

especially with respect to previous simulations including classical MD results [28]. Presence of homopolar As–As and Se–Se bondings in the stoichiometric compound has been, furthermore, found [27] (figures 1(b) and (d)), and also a dendritic network containing a smaller presence of rings [18] as compared to other chalcogenides (e.g. GeSe_2). Finally, the simulations have been able to qualitatively reproduce the electronic structure (valence and conduction bands), consistently with previous findings [29] and compatible with experiments using x-ray photoelectronic spectroscopy [30].

From the obtained structural models, a neighbor decomposition is performed, and the comparison with a measured [31] pair correlation function $g(r)$ is reproduced in figure 2.

2.2.2. GeS_2 . The amorphous GeS_2 system consists in $N = 120$ atoms that are also simulated with a BLYP functional. Comparison and full analysis of structure functions is given in [24], and a very good agreement with experimental data from neutron or x-ray diffraction [12, 32] is also obtained, a situation that is also valid for other compositions in the Ge–S binary [24]. The obtained structures contain a mixture of four-fold Germanium and two-fold Sulphur with the presence of four- (edge sharing tetrahedra) and six-membered rings, and there is a lower tendency in GeS_2 to form homopolar Ge–Ge bonds, as compared to GeSe_2 [23]. Figure 3(a) shows the decomposition into neighbor distributions up to $N = 20$ neighbors, together with experimental results for the total pair correlation function from x-ray or neutron scattering.

2.2.3. GeTe . Amorphous GeTe ($N = 200$ atoms) is obtained [34] from a Perdew–Burke–Erzernhof functional [35] in conjunction to a DFT-D2 Grimme [36] dispersion term that is

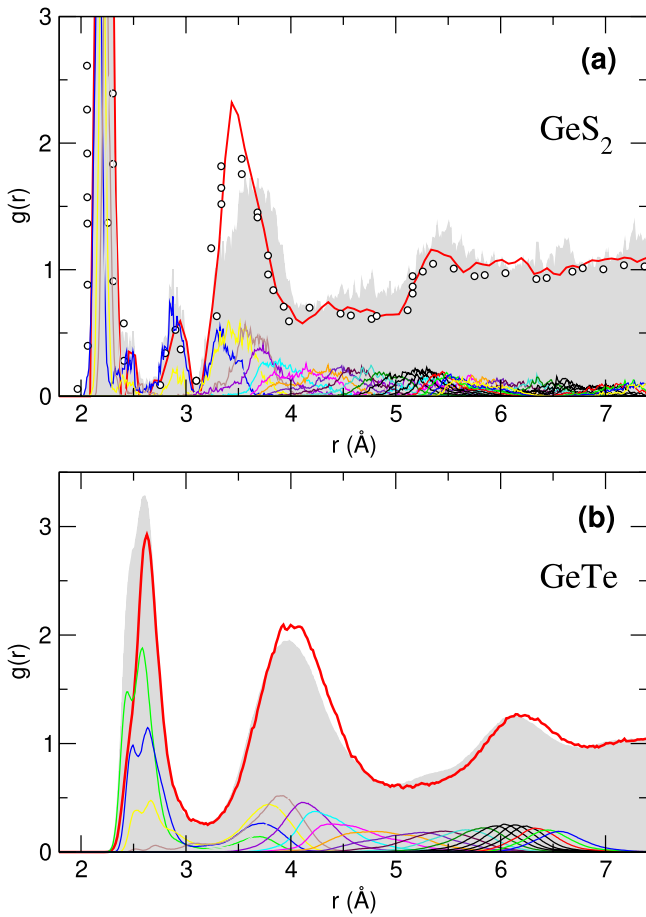


Figure 3. (a) Calculated total pair correlation function $g(r)$ (gray) of simulated amorphous GeS_2 [24] together with its decomposition into neighbor distribution functions $v_n(r)$ (colored curves, up to $N = 10$) and corresponding results from neutron diffraction (red curve, [12]; circles [32]). (b) Calculated total pair correlation function $g(r)$ for amorphous GeTe (gray), compared to experimental data from x-ray diffraction (red curve [33]), and neighbor distribution functions (colored curves).

necessary in order to cure a well-known bond distance problem that occurs in regular DFT simulations of tellurides [37–39]. Such simulations lead, indeed, to an overestimation of Ge–Te bond distances and to an increased population of octahedral geometries. Details of the structural analysis are given in [34]. In short, such dispersion corrected simulations reveal that the Grimme correction reduces the bond length and both $S(k)$ and $g(r)$ are substantially improved with respect to previous regular DFT simulations [40] (figure 3(b)), the spectra from x-ray absorption being also reproduced in an improved fashion [34]. Corresponding neighbor decompositions are provided in figure 3(b). As a result, the structure is made of predominately tetrahedral motifs as in other typical group IV chalcogenides such as GeS_2 .

2.3. Neighbor distribution functions and series expansion

Before checking for the validity of equation (3), we verify that the pair correlation function $g(r)$ can be decomposed into such Gaussian neighbour functions v_n . Figures 2 and 3 show the calculated pair correlation functions $g(r)$ obtained

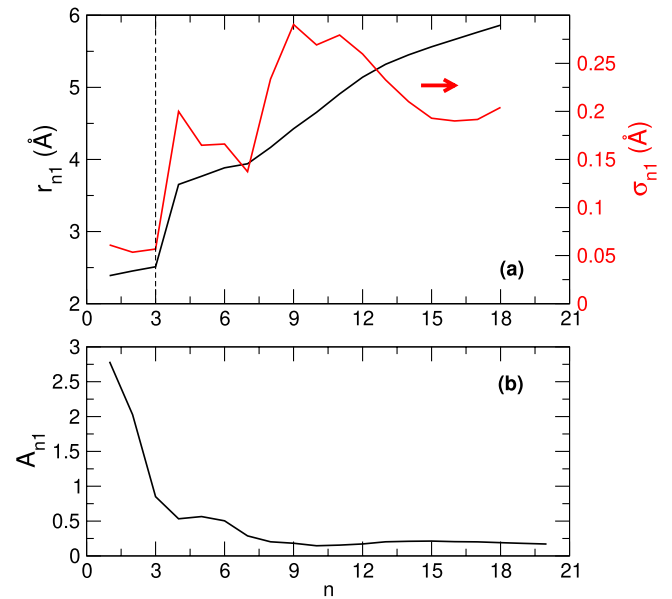


Figure 4. (a) Parameters characterizing the main Gaussian decomposition $m = 1$ in amorphous As_2Se_3 : mean distance r_{n1} and variance σ_{n1} for the main Gaussian decomposition ($m = 1$). The broken line corresponds to $n = 3$ and is linked with the dominant coordination number (As). (b) Amplitudes A_{n1} of the corresponding Gaussian decompositions.

from first principles MD simulations which reproduce, as mentioned earlier, very accurately experimental results from neutron scattering in real space [12, 31–33]. The analysis up to $N = 18$ neighbors shows that corresponding neighbor functions $v_n(r)$ can be decomposed into Gaussian distributions with both r_{nm} and σ_{nm} increasing with n (As_2Se_3 , figure 4(a)), and a sharp increase for both quantities at $n = 3$ signals the 3-fold coordinated As based network structure [22]. For larger n , r_{n1} scales linearly with n with an increment of 0.083 \AA . Such parameters are then used to recalculate the total structure factor using equation (3). Note that because there is an overlap between the different functions $v_n(r)$, at fixed N the decomposition of $g(r)$ is only valid up to $r = r_{\max}(N)$ (broken curve figure 2). For a fixed N and $r > r_{\max}(N)$, additional neighbors are indeed missing ($N + 1, N + 2, \dots$) in order to have exactly $g(r) = \sum_n v_n(r)$, and this defines a minimal momentum transfer $k_{\min} = 2\pi/r_{\max}$ for the validity of equation (3).

Figure 5 now shows the obtained results for amorphous As_2Se_3 with increasing N for the interference function $I(k)$. The latter permits to highlight the oscillations at large momentum transfer in order to check for the accuracy of the series expansion (equation (3)). Quite obviously, a single neighbor decomposition $N = 1$ (using the parameters given in figure 4) leads only to a poor reproduction of $I(k)$, including the oscillations at large k . It is, indeed, also important to note that $I_1(k)$ and the experimental $I(k)$ have a slightly different periodicity at large k ($2.43(5)$ versus $2.78(0) \text{ \AA}^{-1}$). Instead, equation (3) reveals that such high k oscillations can be only obtained (i) for multiple Gaussians having slightly different mean distances r_{nm} and (ii) when the number of Gaussians satisfies $N.M = z$, z being related to the coordination number of the system and determined from the number of functions

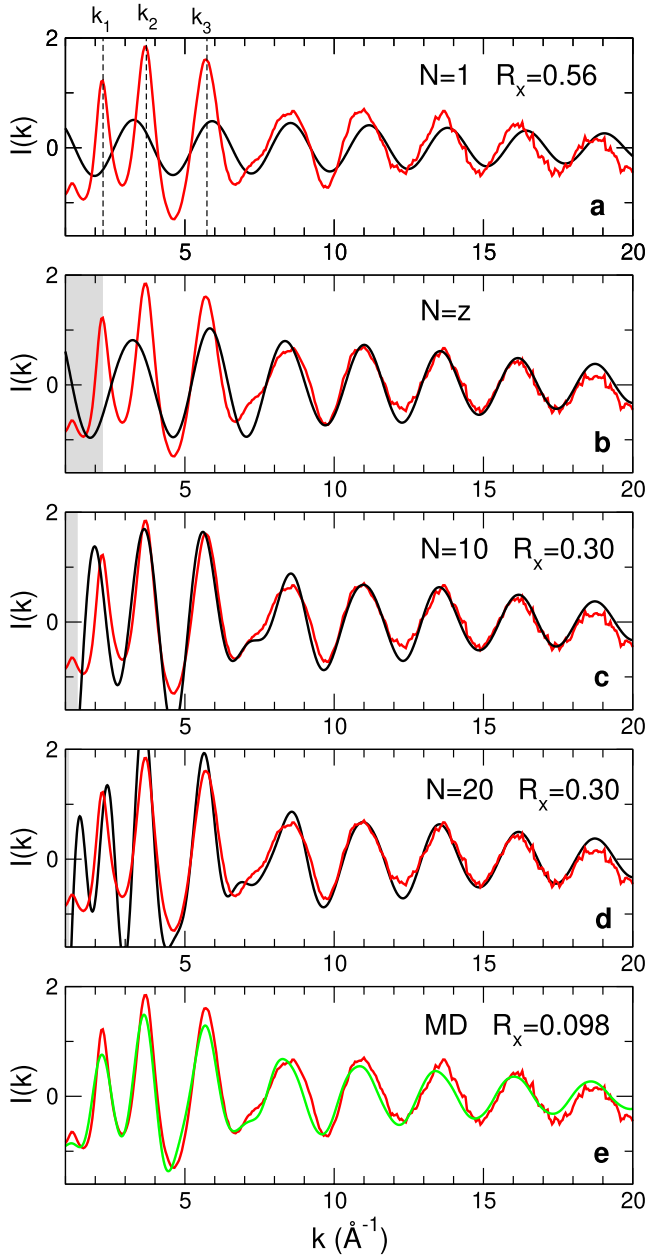


Figure 5. Reconstructed interference function $I(k) = k[S(k) - 1]$ (black curves, (a)–(e)) for increasing number N of neighbor distributions in amorphous As_2Se_3 , using equation (3) (red curves, exp. data [31]). The green curve in panel (e) corresponds to a calculated structure factor from MD simulations [22] using equation (1). For As_2Se_3 , one has $z = 3$ neighbors around a central As atom. Gray zones associated with the main peaks are discussed in the text. The numbers R_x represent the value of the Wright parameter (see text) which measures the degree of accuracy of equation (3).

$u_{nm}(r)$ found for $r < r_{\min}$ with r_{\min} the first minimum of $g(r)$ (three in figure 2, i.e. $u_{11}(r)$, $u_{12}(r)$, $u_{13}(r)$). In the present case, a calculation of the coordination number \bar{n} from such functions using the condition $N.M \leq z$ leads to $\bar{n} = 2.33$ which is compatible with experiments ($\bar{n} = 2.30$ [31]). One also notices that for $k > 7 \text{ \AA}^{-1}$ any further evolution with increasing N is barely visible up to $N = 20$ (figure 5), the contributions $I_n(k)$ with larger n in this range of momentum transfer leading to $I_n(k) \simeq 0$ (see below, and figure 6). This results from the

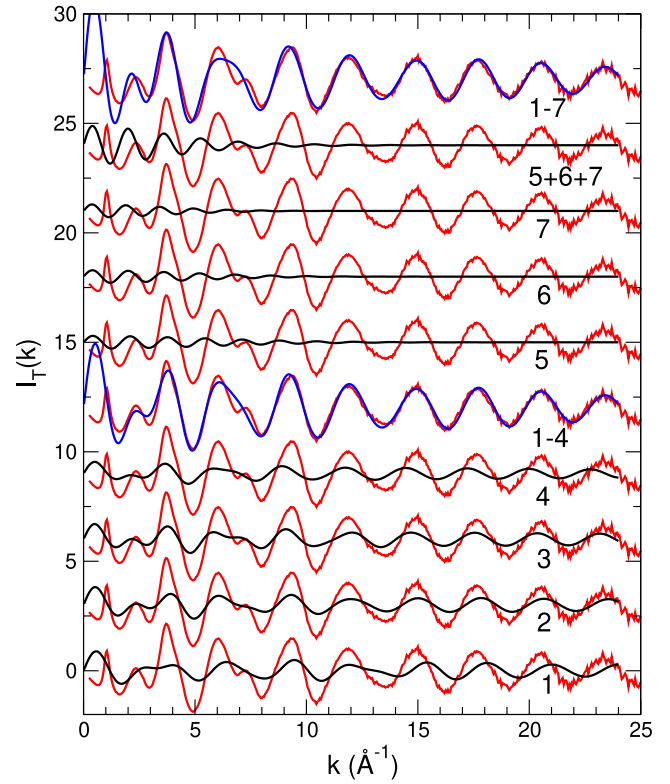


Figure 6. Components $I_n(k)$ for various n (black curves) of amorphous GeS_2 , compared to the experimental function $I(k)$ (red curves [12], duplicated). Blue curves represent $I_1 + I_2 + I_3 + I_4$ and $I(k)$ for $N = 7$ (top). For $n > z$, at large k , one has $I_n(k) \rightarrow 0$.

mathematical properties of the Fadeeva function which lead to (i) $L_{nm} \gg V_{nm}$ for the considered parameters and range of momentum transfer k , and (ii) to a rapid decay to zero of L_{nm} with k , this effect being even enhanced with increasing σ_{nm} and this happens with the dramatic jump obtained between first and second shell of neighbors, e.g. at $n = 3$ for σ_{n1} (figure 4(a)). As a consequence, we arrive to the mathematical conclusion that the large k behaviour of $S(k)$ is dominated by the first coordination shell or SRO of the system.

The qualitative relationship between the behavior of $I(k)$ in the high- k sections and SRO has been long known, as emphasized in reference textbooks [13, 41] but not quantified mathematically. In this respect, several authors [1, 11] have attempted to rescale the diffraction pattern as a function of kr_1 with r_1 the first interatomic neighbor distance. Here, it should be emphasized that the obtained explicit dependence (equation (3)) goes well beyond such qualitative statements found in such textbooks. An expansion of equation (3) in the high momentum transfer given below indicates, indeed, that $I(k)$ has a non-trivial mathematical form that helps decoding experimental diffraction patterns, as discussed below.

3. Analysis of typical glasses

Using the series expansion, it is now insightful to analyze the experimental diffraction pattern [31] with growing N in order to extract information on SRO and IRO elements, and to examine the convergence properties of equation (3).

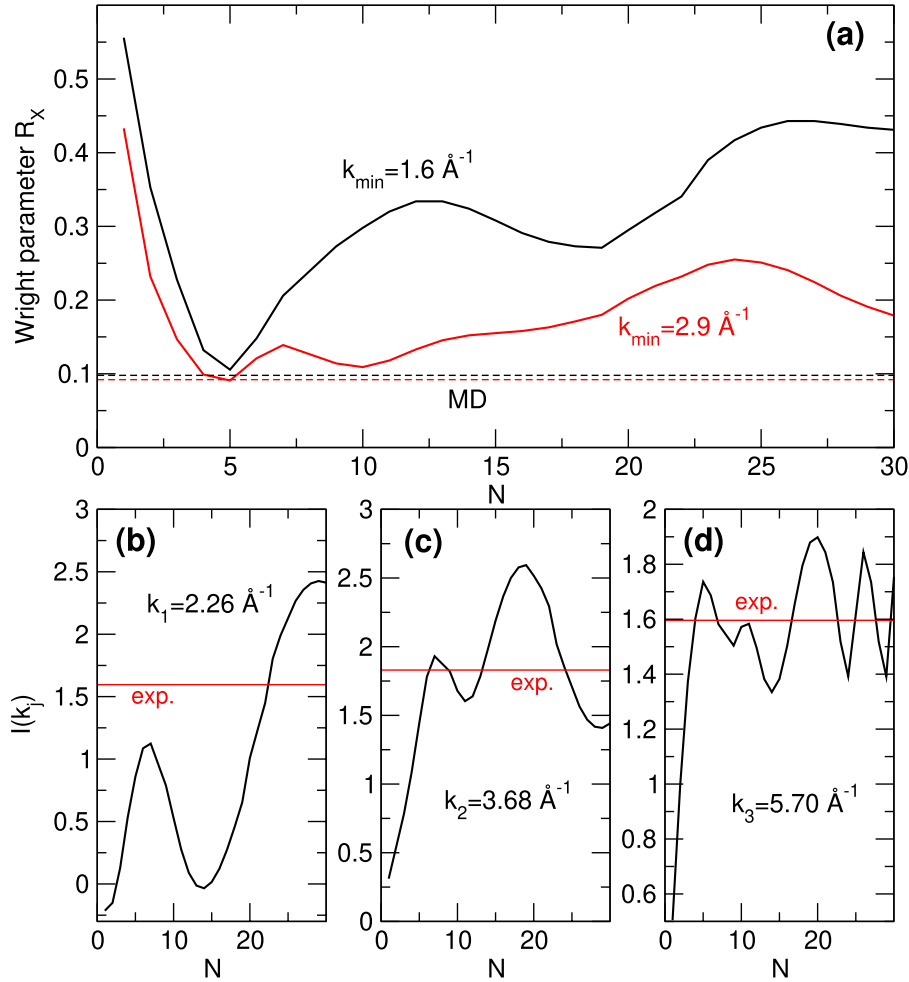


Figure 7. (a) Wright parameter in As_2Se_3 as a function of the number N of considered neighbor distributions using as lower limit for equation (7) $k_{\min} = 1.6 \text{ \AA}^{-1}$ (black curve) and 2.9 \AA^{-1} (red curve)). The latter value corresponds to the minimum between the two PP's at k_1 and k_2 (figure 5). Horizontal broken lines represent the corresponding Wright parameter for the MD simulation. Intensity of the main peaks $I(k_1)$ (b), $I(k_2)$ (c) and $I(k_3)$ (d) (see definition in figure 5 top axis) as a function of the neighbor number N . The horizontal line corresponds to the experimental measurement [12].

3.1. As_2Se_3

We find that the PP region ($2\text{--}5 \text{ \AA}^{-1}$) depends substantially on N (see below), a near convergence being achieved for $N \simeq 30$ for larger k , and $I(k)$ has then a profile that is similar to the one calculated from MD [22], albeit the secondary PP at $k_2 = 3.5 \text{ \AA}^{-1}$ is already correctly reproduced (position, amplitude) for $N = 10$ (see also figure 7). The decomposition also reveals that a typical shoulder peak observed at 7.2 \AA^{-1} can be unambiguously assigned with second shell correlations because it is absent for $N < z$, has a significant contribution for $4 < n < 7$ and becomes negligibly small for larger n . A standard means quantifying more precisely the accuracy of the approach builds on the Wright parameter R_x which evaluates a squared deviation between experimental ($S_{\text{exp}}(k_i)$) and theoretical data ($S_{\text{calc}}(k_i)$) [42]:

$$R_x = \frac{\sum_i \left[S_{\text{exp}}(k_i) - S_{\text{calc}}(k_i) \right]^2}{\sum_i S_{\text{exp}}^2(k_i)}. \quad (7)$$

Corresponding numbers are given in figure 5 for select N , and the evolution $R_x(N)$ is, furthermore, given in figure 7. Here, the increase of N leads to a global decrease of R_x , although strongly non-monotonic, and indicates that the accuracy of equation (3) should improve with growing N , the convergence being however limited because a correct calculation of the neighbor distribution functions is constrained by both $r_{\text{max}}(N)$ and the distance $L/2$ with L the simulation box size (e.g. $L/2 = 8.87 \text{ \AA}$ and $r_{\text{max}}(N = 30) = 6.64 \text{ \AA}$ for As_2Se_3). Interestingly, a first optimal convergence of equation (3) with respect to the MD result is obtained when first and second shell correlations are considered only ($N \simeq 5$, figure 7), as also observed qualitatively for another system (GeS_2 , figure 6). For such expansions, the quality of the obtained $S(k)$ is of the same level as the MD calculated function (broken curves in figure 7). When the detail of the main peaks is analyzed as a function of the order N of the expansion, it can be furthermore remarked that the first PP at $k_1 = 2.26 \text{ \AA}^{-1}$ probably needs more than 30 neighbor distributions in order to be fairly reconstructed and this statement holds to a lesser extent for the secondary PP (at $k_2 = 3.68 \text{ \AA}^{-1}$)

(figures 7(b) and (c)). On the other hand, the intensity of the third prominent peak at $k_3 = 5.70 \text{ \AA}^{-1}$ is obviously related to first neighbor shell atoms ($N \leq 20$) given that equation (3) reproduces $I(k_3)$ starting from $N = 5$ but with strong oscillations (figure 7(d)), that tend to decrease once each component of the series expansion is examined individually (see e.g. the contribution at $k_3 \simeq 6 \text{ \AA}^{-1}$ in figure 6).

As a final comment, one should note that one has $r_{\max} = 5.64 \text{ \AA}$ for $N = 20$ (yielding $k_{\min} = 1.1 \text{ \AA}^{-1}$). The reproduction of the FSDP region ($\simeq 1.5 \text{ \AA}^{-1}$) might be investigated but important oscillations should remain for each contributions n ($n \leq 20$) as for the PP's so that a near convergence of equation (3) is not achieved for this range of momentum transfer. This is also highlighted from the rather different evolution of the Wright parameter R_X (figure 7(a)) with the chosen momentum transfer range (either $k > k_{\min} = 1.60 \text{ \AA}^{-1}$ or 2.9 \AA^{-1} (red curve)). Indeed, an increased convergence is achieved if a reduced k -range is chosen. This, once again, simply signals that the obtained expression (equation (3)) works well at high k for a limited number N of neighbors but can only be expanded with confidence to lower k with increased N .

3.2. GeS₂ and GeTe

The degree of generality of equation (3) can now be verified for other systems such as amorphous GeS₂ and GeTe. Figure 8 shows the obtained results for the interference function $I(k)$ for two expansions ($N = 4$ and 10). A close inspection reveals that the series expansion (equation (3)) is largely material dependant because a large k domain can be described only from the first neighbors ($N = 4$) in GeS₂ whereas this is not the case for GeTe, this result being compatible with the one obtained for As₂Se₃. Note that the quality of the MD simulations is nearly the same, as detected from the reproduction of the pair correlation function [34] (figure 3). However, the slight shift between theory and experiments occuring at large k in a-GeTe is indicative of the well-known bond length mismatch as theory usually overestimates the Ge–Te bond distance [34] with respect to experiments [33]. For this system, the two peaks of the PP region ($1.8\text{--}4 \text{ \AA}^{-1}$) is conveniently described by second shell neighbor distributions ($N = 10$).

4. The reverse approach

So far, we have essentially built on approaches which use MD generated structural models to obtain a behavior of $S(k)$. For a large number of materials however, such models are either unavailable or of poor quality. Having validated the series expansion from the different previous examples and identified the limitations, we, therefore, now attempt to extract structural information from the analysis of select experimental structure factors. In this respect, the behavior of the function $S(k)$ in the large k limit permits to reduce the number of possible fitting parameters (i.e. r_{nm} , A_{nm} , σ_{nm}), and the accuracy in this range has been verified.

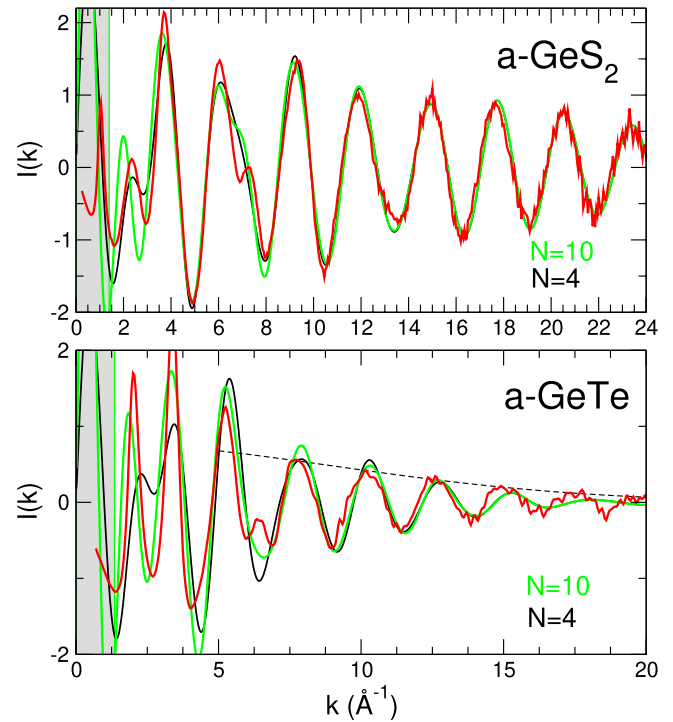


Figure 8. (a) Reconstructed interference functions $I(k)$ (red curves, exp. data) in amorphous (a) GeS₂ (neutrons, [12]), (b) GeTe (x-rays [33]) with variable N (black and green curves). The gray zone corresponds to $k < k_{\min} = 2\pi/r_{\max}$. The broken line is an exponential decay $\exp[-k^2\sigma^2/2]$ with $\sigma = 0.12$ (see text).

4.1. Large k limit

An exact expression for the high momentum transfer limit can be obtained by performing an expansion (appendix) of the Fadeeva function [20] (equation (3)) at $k \rightarrow \infty$, and $I_n(k)$ behaves as:

$$I_n(k) \simeq 8\pi\rho_0\sqrt{2} \sum_m A_{nm}r_{nm}\sigma_{nm}e^{-k^2\sigma_{nm}^2/2} \sin kr_{nm} \quad (8)$$

where the terms beyond the first shell are negligible because of the jump increase of σ_{nm} , as also exemplified from figure 6 where $I_n(k) \rightarrow 0$ at large k . Equation (8) can now serve for the detailed analysis of the SRO of glasses for which no MD generated structural model is available.

In order to obtain information on the SRO from an appropriate fitting using equation (8), we restrict the analysis of experimental functions using equation (8) to $k > 10 \text{ \AA}^{-1}$. The methodology is the following: we assume that σ_{n1} is nearly constant for the first shell of neighbors ($\sigma_{n1} \simeq \sigma$, see e.g. figure 4(a)). We fit the high- k behavior with an increasing number (n, m) of Gaussians and repeat the procedure until (i) any additional Gaussian does not modify the obtained fit and in practice one will have $A_{nm} \simeq 0$ for such additional Gaussians, and (ii) the correlation coefficient r of the fit is fully converged and does not change upon any additional Gaussian. Results for select functions are shown in figure 9 and additional information is provided in table 1. These results reveal that an analysis of the high- k behavior permits one to extract more than a typical bond length that can be compared to experimental results

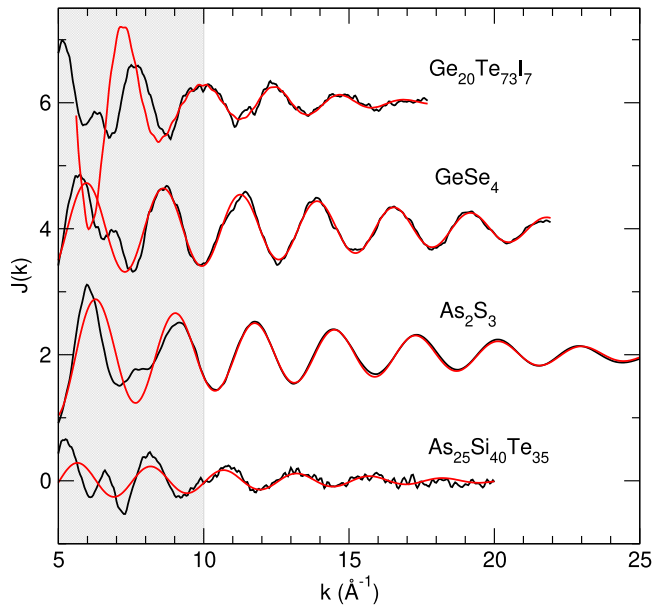


Figure 9. Rescaled experimental interference function $J(k) = I(k)/8\pi\rho_0\sqrt{2}$ (black) for select glass-forming systems ($\text{As}_{25}\text{Si}_{40}\text{Te}_{35}$ [43], As_2S_3 [45], GeSe_4 [48], $\text{Ge}_{20}\text{Te}_{73}\text{I}_7$ [50]) together with the fit using equation (8) (red curves). The fit applies only to the range $k > 10 \text{ \AA}^{-1}$, and curves have been shifted upwards by multiples of 2.

obtained after e.g. a reverse Monte Carlo (RMC) modelling [43–45, 47–50] of the experimental x-ray scattering function. For instance, it is found that As–S glasses contain three typical bond distances at 2.23–2.26 Å, 2.34–2.38 Å and 2.16 Å that can be associated with As–S, As–As and S–S bond distances, respectively (table 1). A similar conclusion holds for GeSe_4 and the fit provides bond distances of Ge–Se and Se–Se, the homopolar Ge–Ge being absent in this compound [48]. The same analysis can be performed for ternary glasses (As–Si–Te [43], Ge–As–Se [49] or Ge–Te–I [50]) that permits to infer bond distances without need of a numerical model from RMC or MD.

An important result of equation (8) links the exponential decay $\exp -k^2\sigma^2/2$ of the interference function (see figure 9) with the parameter σ which provides information on the spatial extent of the neighbor distributions and also a measure of the rigidity of the SRO geometrical units because a small σ value will induce a small bond variability. Qualitatively, the decay of $I(k)$ for amorphous GeTe (figure 8) can now be associated with the presence of more softer units which leads to larger values for σ as also independently verified from the calculated Ge-centred bond angle distribution which exhibits a broader distribution around 109° , as compared to selenides or sulphides [34]. An inspection of table 1 indicates, indeed, that this general feature is also recovered for other glassy materials because one has σ systematically greater by a factor of two in tellurides, as compared to Se- and S-based glasses.

Another compact form can be derived for the high k -limit by assuming that $A_{n1} \simeq A$, and one obtains from equation (8):

$$I(k) \simeq 8\sqrt{2}\pi\rho_0A\sigma e^{-k^2\sigma^2/2} \frac{d}{dk} \frac{\cos k\bar{r} \sin kza}{\sin \frac{ka}{2}} \quad (9)$$

Table 1. Fitting parameters (σ , r_{nm} and correlation parameter r) used in equation (8) applied to different glasses, and compared to possible bond distances r_{ij}^{exp} (measured or reverse Monte Carlo calculated) with identified interatomic bonds.

System	σ (Å)	r_{nm} (Å)	r_{ij}^{exp} (bond) (Å)	r
$\text{As}_{25}\text{Si}_{40}\text{Te}_{35}$	0.101	2.39	2.38 (Ge–Te [43])	0.86
		2.53		
As_2S_3	0.042	2.23	2.26 (As–S [44])	0.99
		2.34		
AsS_2	0.077	2.16	2.18 (S–S [24])	0.99
		2.26	2.26 (As–S [45])	
		2.38	2.40–2.46 (As–As [46])	
GeSe_4	0.078	2.16	2.18 (S–S [24])	0.99
		2.34	2.32 (Se–Se [47])	
$\text{Ge}_5\text{As}_{10}\text{Se}_{85}$	0.037	2.39	2.37 (Ge–Se [48])	0.99
		2.32	2.34 (Se–Se [49])	
		2.43	2.40 (As–Se [49])	
$\text{Ge}_{20}\text{Te}_{73}\text{I}_7$	0.123	2.57	(2.58 (Te–I [50]))	0.94
		2.63	(2.60 (Ge–Te [50]))	
		2.68	(2.70 (Te–Te [50]))	

Table 2. Calculated average distance \bar{r} using the explicit periodicity Λ of the large k behavior of $I(k)$ (see text), determined for different amorphous and liquid materials. It is compared to the bond distance d determined from the principal peak position of the experimental pair correlation function $g(r)$.

System	\bar{r} (Å)	d (Å)	Reference
a- As_2Se_3	2.37 ± 0.17	2.39	[31]
a- GeS_2	2.22 ± 0.16	2.21	[12]
a- GeSe_2	2.32 ± 0.04	2.36	[11]
a- GeTe	2.66 ± 0.07	2.61	[33]
l- GeTe_4 (820 K)	2.68 ± 0.04	2.73	[37]
l- H_2O (300 K)	2.80 ± 0.15	2.81	[51]
l- Te (623 K)	2.68 ± 0.05	2.77	[16]

where one has assumed that r_{n1} increases linearly in the first shell ($r_{n1} = r_0 + na$, figure 4(a)) where a is a bond distance increment (typically $a = 0.06 \text{ \AA}$) and $\bar{r} = z^{-1} \sum_{n=1}^z r_{n1}$ is the average bond distance. Given the value of the different atomic parameters, the arguments of the trigonometric functions have the property $za \ll \bar{r}$ so that the periodicity Λ of the interference function at large k is dominated by $\Lambda = 2\pi/\bar{r}$ and connects to the SRO characteristics (average first neighbor distance) of the material. Corresponding results determined from experimental data are given in table 2 and provide a good agreement with the distances d that are directly obtained from the principal peak position of the measured pair correlation function $g(r)$. The modulation in equation (9) has a periodicity of $\Lambda_m = \pi/2za \gg \Lambda$ which provides a measure of both the coordination number and a but such a modulation is barely visible from the considered k range (figure 9). Using equation (9), a fit to the data at large k at the maximum of the oscillations up to the maximal available k -range ($\simeq 20\text{--}35 \text{ \AA}^{-1}$) [12, 31, 33] permits to analyze the exponential decay and leads to $\sigma = 0.098 \text{ \AA}$, 0.063 \AA , 0.12 \AA for As_2Se_3 , GeS_2 ,

GeTe respectively, smaller than the one performed on the experimental data of water ($\sigma = 0.163 \text{ \AA}$, [51]). An increased exponential decay of $I(k)$ (equation (9)) is, indeed, visible in the liquid state [16, 37, 51], and is driven by the larger value of σ induced by the increased atomic motion which broadens the typical peaks of the pair correlation function.

4.2. Low k limit

In the low k limit, a similar expansion of equation (3) permits to access to the long wavelength limit ($k \simeq 0$) and $S(k)$ that can be expanded from equations (3) and (4).

$$S(0) \simeq 1 + \frac{8\rho_0}{\sqrt{\pi}} \sum_{n,m}^N A_{nm} \sigma_{nm}^3 r_{nm} \left(e^{-r_{nm}^2/2\sigma_{nm}^2} + \frac{\sqrt{2\pi}}{\sigma_{nm}} r_{nm} \operatorname{erfc} \left[-\frac{r_{nm}}{\sigma_{nm}\sqrt{2}} \right] \right) \quad (10)$$

with erfc the complementary error function and where, by virtue of the definition of $S(0)$ from number fluctuations [2], it is only valid in the thermodynamic limit ($N \rightarrow \infty$) [52, 53].

5. Summary and conclusion

In summary, we have shown that the numerical decomposition of the pair distribution function into neighbor distribution functions permits to reconstruct the structure factor $S(k)$ as a series expansion, in a fashion that bears similarities with the pioneering work on crystals with weak disorder [7, 8, 13]. The expansion builds on the Fadeeva functions and contains parameters which characterize the structure, i.e. typical bond distances r_{nm} and their radial excursions σ_{nm} .

Results not only indicate that a few shells of neighbors ($\simeq 20$ atoms) are sufficient in order to describe $S(k)$ over extended ranges in momentum transfer with an obvious increased accuracy achieved at large k , they also provide a direct link between typical features observed in reciprocal space and the neighbour rank (i.e. N) which should certainly help for an improved analysis of experimental diffraction patterns of glasses. The reverse application is explored for different chalcogenide glasses and a fit to the high k limit of the Fadeeva expansion permits to extract typical bond distances, the radial excursion leading to an exponential decay of $I(k)$ that is enhanced in glasses with increased non-directional bonding (tellurides) and in liquids. Finally, given the rather high degree of generality of the expansion, it would be interesting to probe its applicability to other materials including metallic glasses or stable liquids, or even probe how partial correlations from isotopic neutron scattering or anomalous x-ray scattering could be decoded using these methods.

Acknowledgments

The author thanks C Benmore, E Bychkov, L Cormier, G J Cuello, P S Salmon, P J v ari and A Zeidler for useful discussions and for sharing their experimental data. French HPC

Center ROMEO of Universit  Reims Champagne-Ardenne is acknowledged for supercomputing access.

Appendix

The dominant term of the interference function found in equation (3) is equal to:

$$I(k) = 4\pi\rho_0 \sum_n A_{nm} \sigma_{nm} \sqrt{2} e^{-r_{nm}^2/2\sigma_{nm}^2} r_{nm} L_{nm} \quad (A.1)$$

with L_{nm} the imaginary part of the Fadeeva function $w(x, y)$ given in equation (6).

The proposed expansion (equation (8)) builds on a derivation by Abrarov and Quine [20] which have shown that the complex error function in the limit ($x, y \ll 1$) writes:

$$w(x, y) \simeq e^{(ix-y)^2} \left[1 + \frac{2i}{\sqrt{\pi}} e^{x^2} F(x) - \frac{i}{x\sqrt{\pi}} e^{x^2} \left(1 - e^{2ixy} \right) \right] \quad (A.2)$$

with $F(x)$ the Dawson function defined by:

$$F(x) = \frac{1}{2} \int_0^\infty e^{-u^2/4} \sin(xu) du. \quad (A.3)$$

For large x (i.e. k), the Dawson integral reduces to:

$$F(x) \simeq \frac{1}{2x} + \frac{1}{4x^3} \quad (A.4)$$

and the corresponding imaginary part of the Fadeeva function is then equal to:

$$L(x, y) = \frac{e^{y^2}}{x\sqrt{\pi}} - e^{y^2-x^2} \sin(2xy). \quad (A.5)$$

ORCID iDs

M Micoulaut  <https://orcid.org/0000-0002-0273-0563>

References

- [1] Fischer H E, Barnes A C and Salmon P S 2006 *Rep. Prog. Phys.* **69** 233
- [2] Hansen J P and McDonald I R 2006 *Theory of Simple Liquids* (Amsterdam: Elsevier)
- [3] Steimer C, Coulet M-V, Welnic W, Dieker H, Detemple R, Bichara C, Beuneu B, Gaspard J-P and Wuttig M 2008 *Adv. Mater.* **20** 4535
- [4] Kohara S and Salmon P S 2016 *Adv. Phys.* **X** **1** 640
- [5] Cliffe M J, Dove M T, Drabold D A and Goodwin D L 2010 *Phys. Rev. Lett.* **104** 125501
- [6] Pandey A, Biswas P and Drabold D A 2016 *Sci. Rep.* **6** 33731
- [7] Warren B E 1937 *J. Appl. Phys.* **8** 645
- [8] Bernal J D and Fowler R H 1933 *J. Chem. Phys.* **1** 515
- [9] Elliott S R 1991 *Nature* **354** 445
- [10] Bychkov E, Benmore C J and Price D L 2005 *Phys. Rev. B* **72** 172107
- [11] Salmon P S, Martin R A, Mason P E and Cuello G J 2005 *Nature* **435** 75
- [12] Zeidler A, Drewitt W E, Salmon P S, Barnes A C, Crichton W A, Klotz S, Fischer H E, Benmore C J,

- Ramos S and Hannon A C 2006 *J. Phys.: Condens. Matter* **21** 474217
- [13] Guinier A 1963 *X-Ray Diffraction* (London: W.H. Freeman)
- [14] Kakinoki J, Katada K, Hanawa T and Ino T 1960 *Acta Crystallogr.* **13** 171
- [15] Micoulaut M, Otjacques C, Raty J-Y and Bichara C 2010 *Phys. Rev. B* **81** 174206
- [16] Akola J, Jones R O, Kohara S, Usuki T and Bychkov E 2010 *Phys. Rev. B* **81** 094202
- [17] Raty J-Y, Otjacques C, Gaspard J-P and Bichara C 2010 *Solid State Sci.* **12** 193
- [18] Bauchy M, Kachmar A and Micoulaut M 2014 *J. Chem. Phys.* **141** 194506
- [19] Penner S 1959 *Quantum Molecular Spectrum and Gas Emissivities* (Reading, MA: Addison-Wesley)
- [20] Abrarov S M and Quine B M 2014 *J. Math. Res.* **7** 44
- [21] Car R and Parrinello M 1985 *Phys. Rev. Lett.* **55** 2471
- [22] Bauchy M, Micoulaut M, Boero M and Massobrio C 2013 *Phys. Rev. Lett.* **110** 165501
- [23] Micoulaut M, Kachmar A, Bauchy M, Le Roux S, Massobrio C and Boero M 2013 *Phys. Rev. B* **88** 054203
- [24] Chakraborty S, Boolchand P and Micoulaut M 2017 *Phys. Rev. B* **96** 094205
- [25] Becke A D 1988 *Phys. Rev. A* **38** 3098
- Lee C, Yang W and Parr R G 1988 *Phys. Rev. B* **37** 785
- [26] Bauchy M 2013 *J. Non-Cryst. Solids* **377** 39
- [27] Bauchy M and Micoulaut M 2013 *J. Non-Cryst. Solids* **377** 34
- [28] Mauro J C and Varshneya A K 2007 *J. Non-Cryst. Solids* **353** 1226
- [29] Drabold D A, Li J and Nyago Tafen D 2003 *J. Phys.: Condens. Matter* **15** S1529
- [30] Hosokawa S, Goldbach A, Boll M and Hensel F 1999 *Phys. Status Solidi B* **215** 785
- [31] Xin S, Liu J and Salmon P S 2008 *Phys. Rev. B* **78** 064207
- [32] Bychkov E, Miloshova M, Price D L, Benmore C J and Lorriaux A 2006 *J. Non-Cryst. Solids* **352** 63
- [33] Ghezzi G E, Raty J-Y, Maitrejean S, Roule A, Elkaim E and Hippert F 2011 *Appl. Phys. Lett.* **99** 151906
- [34] Micoulaut M, Piarristeguy A, Flores-Ruiz H and Pradel A 2017 *Phys. Rev. B* **96** 184204
- [35] Perdew P, Burke K and Ernzerhof M 1996 *Phys. Rev. Lett.* **77** 3865
- [36] Grimme S 2006 *J. Comput. Chem.* **27** 1787
- [37] Micoulaut M, Coulet M-V, Piarristeguy A, Johnson M R, Cuello G J, Bichara C, Raty J-Y, Flores-Ruiz H and Pradel A 2014 *Phys. Rev. B* **89** 174205
- [38] Micoulaut M 2013 *J. Chem. Phys.* **138** 061103
- [39] Flores-Ruiz H, Micoulaut M, Coulet M-V, Piarristeguy A, Johnson M R, Cuello G J and Pradel A 2015 *Phys. Rev. B* **92** 134205
- [40] Kalikka J, Akola J, Jones R O, Kohara S and Usuki T 2012 *J. Phys.: Condens. Matter* **24** 015802
- [41] Egami T and Billinge S L 2012 *Underneath the Bragg Peaks* (New York: Pergamon)
- [42] Wright A C 1993 *J. Non-Cryst. Solids* **159** 264
- [43] Kaban I, Gruner S, J v ri P, Kehr M, Hoyer W, Delaplane R G and Popescu M 2007 *J. Phys.: Condens. Matter* **19** 335210
- [44] Kaban I, J v ri P, Wagner T, Frumar M, Stehlik S, Bartos M, Hoyer W, Beuneu B and Webb M A 2009 *J. Phys.: Condens. Matter* **21** 395801
- [45] Kaban I, J v ri P, W gner T, Bartos M, Frumar M, Beuneu B, Hoyer W, Mattern N and Eckert J 2011 *J. Non-Cryst. Solids* **357** 3430
- [46] Petkova T, Petkov P, J v ri P, Kaban I, Hoyer W, Sch ps A, Webb A and Beuneu B 2007 *J. Non-Cryst. Solids* **353** 2045
- [47] Sen S and Gan Z 2010 *J. Non-Cryst. Solids* **356** 1519
- [48] Massobrio C, Celino M, Salmon P S, Martin R A, Micoulaut M and Pasquarello A 2009 *Phys. Rev. B* **79** 174201
- [49] Kaban I, J v ri P, Wang R-P, Luther-Davies B, Mattern N and Eckert J 2012 *J. Phys.: Condens. Matter* **24** 385802
- [50] J v ri P, Kaban I, Bureau B, Wilhelm A, Lucas P, Beuneu B and Zajac D A 2010 *J. Phys.: Condens. Matter* **22** 404207
- [51] Skinner L B, Galib M, Fulton J L, Mundy C J, Parise J B, Pham V T, Schenter G K and Benmore C J 2016 *J. Chem. Phys.* **144** 134504
- [52] De Graf A M R and Thorpe M F 2010 *Acta Cryst. A* **66** 22
- [53] Barkema G T and Mousseau N 2000 *Phys. Rev. B* **62** 4985